

Broken symmetries in scanning tunneling images of carbon nanotubes

C. L. Kane and E. J. Mele

Department of Physics, Laboratory for Research on the Structure of Matter, University of Pennsylvania, Philadelphia, Pennsylvania 19104

(Received 22 February 1999)

Scanning tunneling images of carbon nanotubes frequently show electron distributions that break the local sixfold symmetry of the graphene sheet. We present a theory of these images that relates these anisotropies to the off-diagonal correlations in the single-particle density matrix, and allows one to extract these correlations from the observed images. The theory is applied to images of the low-energy states reflected at the end of a tube or by point defects, and to states propagating on defect free semiconducting tubes. The latter exhibit a switching of the anisotropy in the tunneling image with the sign of the tunneling bias.

[S0163-1829(99)50920-X]

Scanning tunneling microscopy and spectroscopy is a powerful tool for studying the structural and electronic properties of carbon nanotubes at the atomic scale. Several experimental groups have reported tunneling images of isolated single wall carbon nanotubes^{1,2} and of tubes packed into bundles or “ropes.”³ In some cases these measurements have allowed a direct determination of the diameters and wrapping vectors for the tubes and these observations, combined with scanning tunneling spectroscopy, have confirmed the idea that the semiconducting or conducting behavior of a tube is controlled by its wrapping vector.^{1,2}

However, scanning tunneling microscopy (STM) images of these systems obtained at low bias voltages contain a number of surprising features. At low bias voltages the images rarely display the full sixfold lattice symmetry even when the underlying graphene lattice is undistorted. Instead, these images frequently contain a broken symmetry in the form of “striped” patterns in which maxima in the electron density are observed in bond chains that spiral around the tube.¹⁻³ In some images superlattice structures are present with a period commensurate with but larger than that of the underlying graphene sheet.⁴ Moreover, energy resolved images of short tubes show standing waves characteristic of individual eigenstates that also have a period longer than that of the graphene lattice.⁵

In special cases broken translational or rotational symmetries obtained in an STM image can be attributed to asymmetries in the tunneling tip.⁶ In this paper we point out that asymmetric images are expected even in an *ideal* tunneling experiment and contain important information about the low-lying electronic states in these systems. The asymmetries are *interference patterns* that are sensitive to the coherence between the “forward” and “backward” moving electronic states propagating on the tube walls. This can arise from backscattering from tube ends, from various defects on the tube walls, and even from propagation in a translationally invariant potential on a semiconducting tube. We show that these interference patterns in the tunneling images are fingerprints that directly probe the off-diagonal correlations in the single-particle density matrix. We provide a theory for extracting these correlations from the observed images. This effect is illustrated with several examples of the tunneling densities of states calculated for defect free tubes and for tubes with point defects.

The low-lying electronic states on a carbon nanotube are derived from the propagating states near the “Fermi points” of an isolated graphene sheet located at the Brillouin-zone corners shown in the lower panel of Fig. 1.^{7,8} There are two inequivalent points that we will refer to as $K=K_0$ and $K'=-K_0$. Wrapping the graphene sheet into a cylinder requires that the electronic wave functions satisfy periodic boundary conditions $\Psi(\vec{r}+\vec{T}_{m,n})=\Psi(\vec{r})$ where $\vec{T}_{m,n}=m\vec{\tau}_1+n\vec{\tau}_2$ gives the wrapping vector around the tube circumference expressed in terms of the two primitive graphite translation vectors $\vec{\tau}_1=(1/2,\sqrt{3}/2)$ and $\vec{\tau}_2=(-1/2,\sqrt{3}/2)$. When

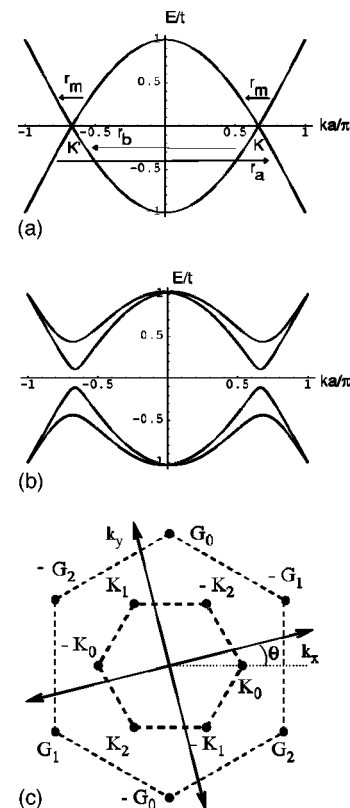


FIG. 1. Low-energy electronic spectra for a conducting tube (a) and for a semiconducting tube (b). The lower panel (c) shows the momenta in the first two stars in reciprocal space that describe the local tunneling density of states in an STM experiment.

$\text{mod}(m-n,3)=0$ the Bloch waves *exactly* at the K and K' points are allowed quantized waves on the tube. This leads to the metallic band structure in Fig. 1(a). In contrast, when $\text{mod}(m-n,3)=(1,2)$ the allowed quantized waves do not intersect K and K', which leads to a semiconducting gap in the electronic spectrum as shown in Fig. 1(b).

The spectrum of Fig. 1(a) describes the propagating modes of a defect free conducting tube. However, these waves can be reflected from tube ends or from defects along the tube. The interference between the forward and backward moving waves produces a spatial modulation of the charge density. Since the carbon nanotubes have two forward and backward moving channels (associated with the K and K' points shown in Fig. 1) the resulting interference patterns have a particularly rich structure. The coherent superposition of the forward and backward moving components of the scattering states produces off-diagonal correlations in the density matrix at energy E ,

$$\rho_{\alpha\beta}(E) = \langle \psi_{\alpha}^{\dagger} \delta(E - \mathcal{H}) \psi_{\beta} \rangle, \quad (1)$$

where \mathcal{H} is the Hamiltonian and α is a four component index specifying the left and right moving bands at the K and K' points.

To derive the local tunneling density of states from the density matrix in Eq. (1) we represent the Bloch waves $\psi_{\alpha}(\vec{r})$ as a sum atomic orbital centered on sites $\vec{\tau}_m$ in cells \vec{T}_n

$$\psi_{\alpha}(\vec{r}) = \sum_{m,n} \gamma_{m\alpha} e^{i\vec{k}_{\alpha} \cdot \vec{T}_n} f(\vec{r} - \vec{\tau}_m - \vec{T}_n), \quad (2)$$

where $\gamma_{m\alpha}$ are the amplitudes for the Bloch state on sites m . These Bloch waves can be represented as an expansion in reciprocal lattice vectors

$$\psi_{\alpha} = \sum_{m,n} \gamma_{m\alpha} e^{-i(\vec{k}_{\alpha} + \vec{G}_n) \cdot \vec{\tau}_m} F(|\vec{k}_{\alpha} + \vec{G}_n|) e^{i(\vec{k}_{\alpha} + \vec{G}_n) \cdot \vec{r}}. \quad (3)$$

For tunneling from a tip that is smooth on a scale of the atomic spacing, $F(q)$ decreases rapidly for large q . In the following we will truncate this expansion, keeping only \vec{G} 's in the lowest "star" of $\vec{k}_{\alpha} + \vec{G}$. This becomes exact when the STM tip is sufficiently high above the surface.⁹ Including higher Fourier components does not significantly change our conclusions. We also assume the tip is isotropic, so within the first star $F(|\vec{k} + \vec{G}|)$ is independent of \vec{G} .

The local density of states at energy E can be expressed

$$\rho(\vec{r}, E) = \psi_{\alpha}^*(\vec{r}) \rho_{\alpha\beta}(E) \psi_{\beta}(\vec{r}). \quad (4)$$

It is useful to characterize the tunneling image in terms of its longest wavelength Fourier components. Coupling between bands at the same K point leads to images with the periodicity of the lattice. These are described by Fourier components in the first star of reciprocal lattice vectors $\vec{q}_{1i} = \vec{G}_i$, indicated in Fig. 1. On the other hand, coupling between the two K points leads to modulations with a $\sqrt{3} \times \sqrt{3}$ superlattice, which are described by the " $\sqrt{3}$ " star, $\vec{q}_{\sqrt{3}i} = \vec{K}_i$. The discussion is further simplified by projecting onto the "triangular harmonics" defined in each star to be

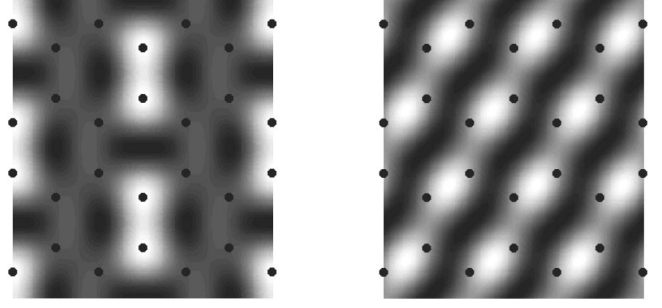


FIG. 2. Local tunneling densities of states for a [10,10] tube in the presence of reflection from point defects. The left panel shows a tunneling image that is modulated in a $\sqrt{3} \times \sqrt{3}$ pattern and the right panel shows a "primitive" 1×1 spiral striped pattern that breaks a mirror symmetry of the armchair tube.

$$\rho_{pm} = \frac{1}{3} \sum_{n=0}^2 e^{2\pi i mn/3} \int d^2r e^{-i\vec{q}_{pn} \cdot \vec{r}} \rho(\vec{r}), \quad (5)$$

with $p=1$ or $\sqrt{3}$ and $m=-1,0,1$. Combining Eqs. (1)–(5) yields a simple expression for the Fourier components $\rho_{pm}(E)$ in terms of the density matrix $\rho_{\alpha\beta}(E)$.

We first consider the effects of reflection either from the end of the tube or from an impurity. The reflection of waves associated with the K and K' points is characterized by a 2×2 matrix of complex reflection amplitudes. This matrix contains three independent amplitudes labeled r_a , r_b , and r_m in Fig. 1(a). These describe, respectively, large momentum scattering from $K \rightarrow K'$, $K' \rightarrow K$, and small momentum scattering at the K and K' points. The equality between the two amplitudes described by r_m follows from time-reversal symmetry. These reflection amplitudes depend on the detailed structure of the scatterer, although for special high symmetry scatterers its form can be constrained by symmetry. In the following, we consider an infinitely long tube, so that the density matrix is diagonal in the basis of scattering states, which are a superposition of incoming and reflected waves.

The large momentum scattering amplitudes r_a and r_b illustrated in Fig. 1 produce a modulation of the tunneling density of states (TDOS) in the $\sqrt{3}$ star. For a conducting tube we find that the TDOS measured at energy E and at a distance x from a point scatterer has the Fourier coefficients¹⁰

$$\rho_{\sqrt{3}0}(E) = \frac{1}{2} N(E) (r_b e^{2iQx} - r_a^* e^{-2iQx}),$$

$$\rho_{\sqrt{3}\pm 1}(E) = \frac{1}{2} N(E) e^{\pm i\theta} (r_b e^{2iQx} + r_a^* e^{-2iQx}), \quad (6)$$

where $N(E)$ is the density of states, $Q = E/\hbar v_F$, v_F is the Fermi velocity, and θ is the chiral angle that orients the zigzag bond direction with respect to the tube axis (i.e., $\theta = 0$ defines a tube with an armchair wrapping). The dependence of the TDOS on r_a and r_b is most clearly seen for tunneling at low bias ($E \approx 0$). The Q dependence in Eq. (5) arises from the fact that the scattered states at nonzero energy are not located precisely at the Fermi points.

As an example in Fig. 2 we display the calculated TDOS

at $E=0$ for the values $r_a=r_b=1$ on an armchair tube. The scattering amplitudes produce a $\sqrt{3}\times\sqrt{3}$ modulation of the tunneling image in which the bond charges are enhanced in a superlattice of bonds oriented along the circumferential direction of the tube. Similar $\sqrt{3}\times\sqrt{3}$ modulations occur in the presence of impurities on the surface of graphite.¹¹ Those patterns follow from the two-dimensional scattering between the K and K' points in the graphite plane.

The small momentum backscattering amplitudes r_m produce *cell periodic* modulations of the TDOS that can nonetheless break the rotational symmetry of the image. These effects are produced by a modulation of the Fourier components of the TDOS in the first star of reciprocal lattice vectors \vec{G}_n shown in Fig. 1. Using the expansion in triangular harmonics in Eq. (5) we find¹⁰

$$\rho_{10}(E) = N(E)(-1 + i\sqrt{3} \operatorname{Re}[r_m e^{2iQx}])$$

$$\rho_{1\pm 1}(E) = \mp iN(E)e^{\pm i\theta} \operatorname{Im}[r_m e^{2iQx}]. \quad (7)$$

Interesting structure in the TDOS is produced by the imaginary part of $\rho_{1\pm 1}$. This generally occurs for any chiral tube with $\theta \neq 0$, but it can *also* occur for a nonchiral armchair tube, $\theta=0$, when the $q \approx 0$ backscattering amplitude r_m develops a nonvanishing imaginary part. This leads to the interference pattern shown in the right panel of Fig. 2, in which a bond density wave is deflected into a spiral pattern around the axis of the armchair tube. We find that a reflection amplitude with this symmetry can be produced by any point defect or end cap which breaks the two sublattice symmetry of the underlying graphene sheet.

Semiconducting tubes with $\operatorname{mod}(m-n,3) \neq 0$ have a gap in the low energy spectrum as shown in Fig. 1(b). This gap arises from a coherent superposition of forward and backward moving components that is required for the wave function to satisfy periodic boundary conditions around the tube waist. Exactly at the band edges one obtains a perfect standing wave that contains an equal admixture of forward and backward propagating waves. Note, however, that the backscattering responsible for these states does not result from reflection from an isolated point defect, but instead arises from the presence of a “mass” operator in the low-energy Hamiltonian⁸ that preserves the lattice translational symmetry, and *breaks* its rotational symmetry. Remarkably, the symmetry of this “mass” term depends sensitively on the wrapping vector and allows one to distinguish $\operatorname{mod}(m-n,3)=1$ from $\operatorname{mod}(m-n,3)=2$ tubes. To do this we define the chiral index $s = (-1)^{\operatorname{mod}(m-n,3)}$. Then we find that the tunneling density of states for a semiconducting tube with chiral index s , chiral angle θ , and gap 2Δ is given by¹⁰

$$\rho_{10}(E) = -N(E) \quad \rho_{1\pm 1}(E) = \pm isN(E)e^{\pm i\theta}\Delta/E. \quad (8)$$

In Fig. 3 we display tunneling densities of states calculated for the band-edge states ($E = \pm\Delta$) on tubes with wrapping indices $[m,n] = [12,7]$, $[14,6]$, and $[17,0]$ (zigzag). These three tubes have a common chiral index $s=1$ and chiral angles that vary between 8.6° and 30° . The band-edge states imaged at positive and negative bias have *complementary* structures, that is, the superposition of the two images gives an image with perfect sixfold symmetry although each image

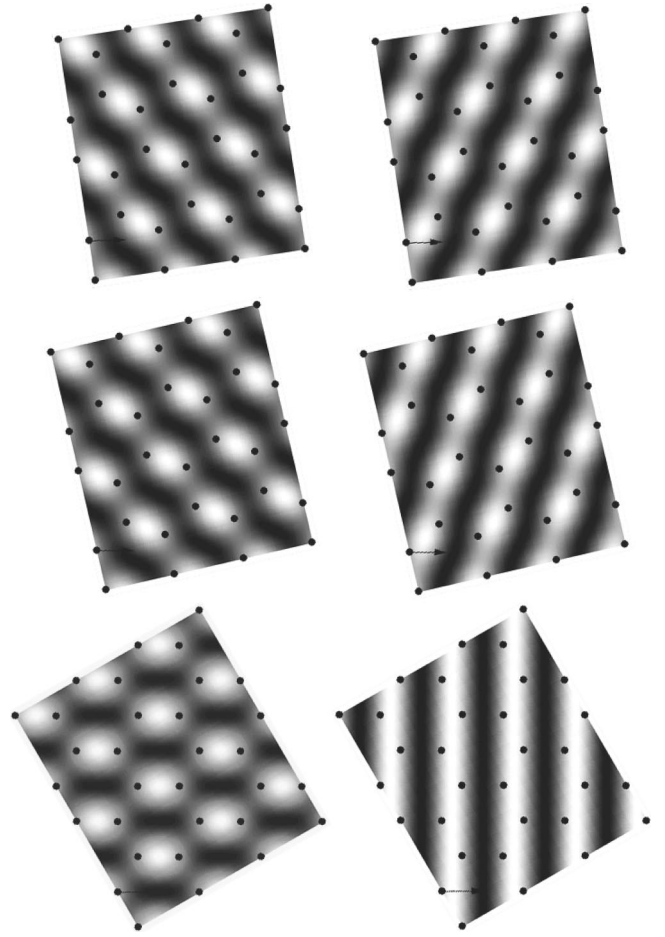


FIG. 3. Complementary tunneling densities of states for the two band edges of three semiconducting chiral tubes with the same chiral index. The left panel gives the image for tunneling into a band-edge state at negative energy ($E = -\Delta$), and the right panel gives the corresponding image at positive energy ($E = \Delta$). The images are for tubes with wrapping indices $[12,7]$ (top), $[14,6]$ (middle), and $[17,0]$ (bottom). In each case the image is rotated so that the tube axis is directed along the horizontal.

separately breaks the sixfold symmetry. For chiral angles near $\theta \approx 0$ the tunneling images consist of a series of complementary spiral stripes. However, the TDOS changes smoothly as a function of chiral angle, so that as one approaches the zigzag structure the negative energy states are enhanced in a pattern of isolated bonds in the structure, while the density for the positive energy states is confined to a connected zigzag bond chain. Note that the symmetry breaking terms in $\rho_{1\pm 1}$ depend on the product of the chiral index *and* the energy. Thus for a $[12,8]$ tube that has a chiral index -1 the symmetries of the positive and negative energy solutions are reversed.

Figure 3 shows that for semiconducting tubes the tunneling images obtained near the band edges break the local point symmetry of the graphene sheet, and that for a given tube the sign of the symmetry breaking is switched by reversing the bias of the tunneling tip. Observation of such a reversal in the tunneling image would provide a striking identification of the chiral index s of a semiconducting tube, even when the wrapping indices $[n,m]$ cannot be resolved. Moreover, this reversal would clearly distinguish this effect

from a tip artifact.⁶ We should note that several experiments have already suggested that a tube in contact with a conducting substrate can be doped “p” type¹ and so one needs to correct such a measurement for the offset in the chemical potential for any such unintentionally “doped” tube. One also needs to ensure that the tunneling is carried out in an energy window where only one azimuthal subband is accessible, since the symmetries of the tube eigenstates alternate in successive conduction or valence subbands, tending to suppress the anisotropy in the tunneling images.

The data presented in Figs. 2 and 3 demonstrate that scanning tunneling images of carbon nanotubes are very sensitive to the nodal structure of the underlying electronic states.⁹ Indeed at low energy these images are probing the internal structure of *individual* (or at best a small number) of electronic eigenstates on the tube surface. The appearance of these broken symmetry patterns in a tunneling image does not imply large structural perturbations to the covalent graphene network. Indeed the data presented here are calcu-

lated for structures that are *all* unstrained and perfectly locally sixfold symmetric. These density patterns do require coherence between forward and backward propagating waves. In fact a quantitative analysis of these images can be used to extract off-diagonal correlations in the density matrix in Eq. (1) responsible for these patterns. These data can then be used to extract the scattering matrix, which characterizes the internal structure and symmetry of various scattering centers, and to identify the wrapping vector for semiconducting tubes. Finally, we remark that the off-diagonal correlations responsible for these patterns could also arise due to interactions with a substrate, interactions between tubes in a rope or due to electron-electron interactions.

It is a pleasure to thank W. Clauss and A.T. Johnson for helpful discussions of their STM images. This work has been supported by the NSF under Grants Nos. DMR 95-05425, DMR 96-32598, and DMR 98-02560, and by the DOE under Grant No. DE-FG02-84ER45118.

¹J.W.G. Wildoer *et al.*, Nature (London) **391**, 59 (1998).

²T.W. Odom *et al.*, Nature (London) **391**, 62 (1998).

³W. Clauss, D.J. Bergeron, and A.T. Johnson, Phys. Rev. B **58**, R4266 (1998).

⁴W. Clauss, D.J. Bergeron, M. Freitag, C. L. Kane, E. J. Mele, and A.T. Johnson (unpublished).

⁵L.C. Venema *et al.*, Science **283**, 52 (1999).

⁶H.A. Mizes, S.I. Park, and W.A. Harrison, Phys. Rev. B **36**, 4491 (1987).

⁷N. Hamada *et al.*, Phys. Rev. Lett. **68**, 1579 (1992); J.W. Mintmire *et al.*, *ibid.* **68**, 631 (1992); R. Saito *et al.*, Appl. Phys. Lett. **60**, 2204 (1992).

⁸C.L. Kane and E.J. Mele, Phys. Rev. Lett. **78**, 1932 (1997).

⁹J. Tersoff, Phys. Rev. Lett. **57**, 440 (1986).

¹⁰To obtain these formulas we specify that the origin $\vec{r}=0$ lies at the center of a hexagon.

¹¹H.A. Mizes and J.S. Foster, Science **244**, 559 (1989).